Hydrogen Isotope Separation in Carbon Nanotubes: Calculation of Coupled Rotational and Translational States at High Densities

Giovanni Garberoglio[†,‡,§,∥,*] **and J. Karl Johnson**[‡,§,*]

[†]CNISM and Dipartimento di Fisica, Università degli Studi di Trento, via Sommarive 14, 38100 Povo (TN), Italy, [‡]Department of Chemical and Petroleum Engineering, University of Pittsburgh, Pittsburgh, Pennsylvania 15261, and [§]National Energy Technology Laboratory, Pittsburgh, Pennsylvania 15236. [∥]Current address: Center for Materials and Microsystems, FBK-IRST, via Sommarive 18, 38100 Povo (TN), Italy.

ABSTRACT The effect of the quantized rotational degrees of freedom of hydrogen on the adsorption and sieving properties in carbon nanotubes is studied using computer simulations. We have developed a highly efficient multiple timestep algorithm for hybrid Monte Carlo sampling of quantized rotor configurations and extended the grand canonical Boltzmann bias method to rigid linear molecules. These new computational tools allow us to calculate accurately the quantum sieving selectivities for cases of extreme two-dimensional confinement as a function of pressure. The *para*-T_2/*para*-H_2 selectivity at 20 K is analyzed as a function of the tube diameter and the density of adsorbed hydrogen. Extraordinarily high selectivities, up to 2.6×10^8, are observed in the narrowest nanotube. The quantized nature of the rotational degrees of freedom is found to dramatically affect adsorption and selectivity for hydrogen isotopes adsorbed in very narrow nanotubes. The T_2/H_2 zero-pressure selectivity increases from 2.4×10^4 to 1.7×10^8 in the (3,6) nanotube at 20 K when quantum rotations are accounted for. The isotopic selectivity is found to increase with pressure, tending to a constant value at saturation. A simplified mean-field model is used to discuss the origin of this behavior.

KEYWORDS: quantum sieving · path integral Monte Carlo · hybrid Monte Carlo · grand canonical Monte Carlo · quantum rotors · isotopic effect · adsorption

Quantum sieving is the name given to the phenomenon by which the various components of an isotopic mixture can be separated by selective adsorption in narrow pores, such as those of single-walled carbon nanotubes (SWNTs).[1−11] The adsorption selectivity is due to the difference in quantum kinetic energy between the isotopes upon adsorption.

The presence of a sizable isotopic effect on surface adsorption has been known since the 1950s,[12,13] and it has been used to efficiently separate *ortho*- from *para*-hydrogen.[14] Although the mechanism for this phenomenon was readily identified as being related to zero-point quantum effects,[15−18] it was only relatively recently that Beenakker *et al.*[1] showed, in the framework of a simple repulsive wall model, the possibility of efficiently separating isotopic mixtures of light gases by making use of the different zero-point energies of the two confined species in very narrow one-dimensional pores.

Various simulation techniques have been employed to investigate quantum sieving in carbon nanotubes, with the aim of understanding how the isotopic selectivity depends on the dimension of the confining SWNT as well as the thermodynamic conditions at which adsorption takes place (that is, the temperature, the isotopic composition of the mixture, and the external pressure).

Path integral Monte Carlo (PIMC) simulations have been shown to be effective for studying adsorption and sieving of hydrogen isotopes under a wide range of conditions. Their use was pioneered by Johnson and collaborators,[2,3] who studied, in particular, the selectivity of T_2/H_2 mixtures inside SWNTs and in the interstitial channels of carbon nanotube bundles. These authors used an interaction potential model that neglects the molecular structure of hydrogen and developed a method to calculate the selectivity in the limit of zero pressure (*i.e.*, neglecting hydrogen−hydrogen interactions) by using the single-particle energy levels in the confined system.[2,3] Their main finding is that the (3,6) nanotube would show a T_2/H_2 selectivity on the order of 10^5 at 20 K. They further calculated the expected selectivities for a wide set of nanotubes, thus describing the dependence of this quantity on the radius of the tubes.

The PIMC technique was later extended to simulate adsorption at finite pressures,[4,10] and the sieving properties of various kinds

*Address correspondence to garberog@science.unitn.it, karlj@pitt.edu.

Received for review November 11, 2009 and accepted January 28, 2010.

Published online February 10, 2010. 10.1021/nn901592x

of carbonaceous pores have been studied with this methodology,[11,19−21] always assuming that hydrogen could be treated as a spherical object.

Hathorn *et al.*[5] were the first to address the effect of the rotational degrees of freedom of hydrogen on the selectivity. Assuming a decoupling of the rotational and translational motions they showed, using a semiclassical approach, that one can expect an increase of the selectivity in narrow tubes by a factor of 100 at 20 K, when compared with models that approximate hydrogen as a sphere. The importance of the rotational degrees of freedom on the selectivity has been confirmed by Trasca *et al.*,[6] who calculated the D_2/H_2 selectivity in the interstitial channels and groove sites of various carbon nanotube bundles, taking into account translational and rotational degrees of freedom in the zero-pressure limit, finding values as high as 10^9 for the D_2/H_2 selectivity in the groove sites of the (18,0) tubes.

Lu *et al.*[7,8] calculated the energy levels and the zero-pressure selectivity of molecular hydrogen in carbon nanotubes by numerical diagonalization of the Schrödinger equation of a confined rotor, finding exceptionally high values—of the order of 10^8, the details depending on the particular solid−fluid potential used—of the total selectivity for T_2/H_2 mixtures at zero pressure and 20 K in the narrow (3,6) tube. The availability of the wave functions for the various eigenstates of hydrogen isotopes confined in carbon nanotubes allowed Lu *et al.* to characterize in detail the origin of these exceptionally high values, and a novel regime of "extreme two-dimensional confinement" (X2DC) was identified. When the dimensions of the confining pores are so small that the molecular rotation is highly hindered, the zero-point energy of the lighter species becomes so high that adsorption is severely hampered. In the case of X2DC, the adsorbed molecules present, in their ground state, a substantial orientational localization along the nanotube axis.

Independent calculations with an approximate treatment of the rotational−translational coupling confirmed the expectation of high selectivity for rotors confined in narrow SWNTs.[9] A phenomenon analogous to X2DC was subsequently predicted and characterized computationally in the case of quantum rotors confined in slit pores.[22]

Although the experimental verification of the large selectivity predicted in narrow SWNTs is still lacking, quantum sieving has been experimentally demonstrated to occur in the case of adsorption in many microporous materials such as carbon nanofibers[23,24] and organic frameworks.[25] In this latter case, the theoretical predictions are in good agreement with experimental results.[26]

TABLE 1. Summary of the Properties of Single Rotors Adsorbed in Nanotubes at $T = 20$ K, Obtained by Direct Diagonalization of the Corresponding Hamiltonian[a]

tube	molecule	SF PE (K)	Tr KE (K)	Rot KE (K)	ΔE (K)	$\tilde{\mu}$ (K)
(3,6)	*para*-H_2	−640 ± 1	303 ± 1	147 ± 1	540.2	−190.5
(3,6)	*para*-T_2	−874 ± 1	159 ± 1	123 ± 1	272.1	−591.7
(2,8)	*para*-H_2	−1234 ± 1	119 ± 1	3.9 ± 0.1	235.7	−1110.4
(2,8)	*para*-T_2	−1277 ± 1	60.2 ± 0.1	6.2 ± 0.1	118.7	−1210.8
(6,6)	*para*-H_2	−998 ± 1	47.1 ± 0.1	0.7 ± 0.1	78.4	−955.2
(6,6)	*para*-T_2	−1005 ± 1	30.6 ± 0.1	0.8 ± 0.1	29.8	−995.6
graphite plane	*para*-H_2	−346 ± 1	41.6 ± 0.1	1.79 ± 0. 01	133	−316
graphite plane	*para*-T_2	−371 ± 1	25.8 ± 0.1	3.59 ± 0. 01	88.8	−356

[a] ΔE is the energy difference between the first excited state and the ground state. SF PE: solid−fluid potential energy. Tr KE: translational kinetic energy. Tot KE: rotational kinetic energy. The translational kinetic energies do not include the contribution from the free motion along the tube axis. All of the observables are calculated as thermal averages; $\tilde{\mu}$ is defined in eq 36.

Finally, we note that recent studies have shown that the transport or membrane selectivity may be enhanced over the adsorption selectivity by the fact that heavier isotopes are found to diffuse more rapidly than the lighter ones in many kinds of microporous materials, a phenomenon known as "quantum kinetic sieving".[27−31]

In this paper, we address the issue of the contribution of coupled rotational and translational degrees of freedom to the isotopic equilibrium selectivity in more detail, combining results from direct diagonalization of the single-particle Schrödinger equation and the PIMC method to investigate the pressure dependence of the selectivity from the free rotational regime (large SWNTs and graphite planes) to the regime of X2DC (narrow SWNTs).

We present the results of calculations at finite pressures and discuss how the selectivity changes in this regime, extending the recently developed Boltzmann bias (BB) method for grand canonical PIMC simulations[10] to the case of rotors adsorbed in narrow pores. The effect of the quantization of the rotational degrees of freedom is analyzed by comparing the full quantum PIMC results with simulations where the rotational degrees of freedom are treated classically (while retaining the full quantum character of the translational degrees of freedom). We provide details on our efficient hybrid Monte Carlo (HMC) path integral simulation technique for quantum rotors. We present the development and characterization of a multiple timestep integrator to sample configuration space efficiently.

RESULTS AND DISCUSSION

Single-Molecule Properties. We report in Table 1 the results obtained by diagonalizing the Hamiltonian describing the interaction of isolated hydrogen isotopes confined in SWNTs and on top of a graphite plane.

First of all, we note that the average translational kinetic energies in the (3,6) and (2,8) SWNTs are much higher than the thermal value that would be expected

for molecules at $T = 20$ K. A careful analysis of the eigenstates reveals that these large values of the kinetic energy are entirely due to the zero-point translational motion of the molecules; the separation ΔE between the ground state and the first excited state, also reported in Table 1, is generally much larger than k_BT in almost all configurations, ranging from 540.2 K in the case of *para*-H_2 in the (3,6) tube to 78.4 K in the case of *para*-H_2 in the (6,6). The only notable exception is that of *para*-T_2 adsorbed in the (6,6) tube, where the excited states are separated by 30 K from the ground state and are therefore thermally occupied with a non-negligible probability.

We also notice that the rotational kinetic energies for H_2 and T_2 in the (3,6) nanotube are much larger than the values that can be expected for free rotors at the same temperatures. In fact, the rotational temperatures for hydrogen and tritium are 88.6 and 29.5 K, respectively, so that the occupation probabilities for the first excited state at $T = 20$ K can be expected to be less than 10^{-3} in the free rotor case, resulting in average rotational kinetic energies very close to 0. On the other hand, the rotational kinetic energies are quite large in the case of adsorption in the narrow (3,6) SWNT. This is indeed an indication that in the ground state of the adsorbed molecules there is a sizable probability of occupation of the rotational states with nonzero angular momentum, which is, according to Lu *et al.*, the characteristic indication of attainment of the X2DC regime. In fact, our calculated first excitation energies ΔE for hydrogen isotopes in the (3,6) tube, reported in Table 1, are comparable to the values assigned by Lu *et al.* to the X2DC regime.

The rotational kinetic energy tends to the free value as the diameter of the SWNT is increased, becoming less than 1 K when both species are adsorbed in the (6,6) tube. In this case, hydrogen and tritium molecules are almost freely rotating, and one might expect a negligible contribution to the selectivity from the rotational degrees of freedom in this case. We note, however, that the (6,6) SWNT is something of a special case, having a flatter potential energy surface than either wider or more narrow nanotubes because of the overlap of the potential from opposite sides of the nanotube, as noted by Challa *et al.*[3] This can also be seen from Table 1, where we report the properties of hydrogen isotopes adsorbed on graphite planes (corresponding to a nanotube of infinite radius). In this case, the rotational kinetic energy of adsorbed isotopes is higher than that in the (6,6) tube, indicating a slightly larger degree of confinement.

The results obtained by direct diagonalization of the Hamiltonian of a single particle adsorbed in a SWNT have been used to check the reliability of the parameters entering the multiple timestep algorithm used for the PIMC simulations, as well as to calculate the value of $\bar{\mu}$ to be used in the BB method, which is also reported in Table 1.

TABLE 2. Zero-Pressure Selectivities for *para*-T_2/*para*-H_2 and Confined *para*-H_2 Observables Calculated for Various Nanotubes at 20 K and Different Methodologies[a]

tube	method	selectivity	SF PE (K)	Tr KE (K)	Rot KE (K)
(3,6)	quantum (DIAG)	1.7×10^8	-640 ± 1	303 ± 1	147 ± 1
(3,6)	quantum (PIMC)	$(1.5 \pm 0.3) \times 10^8$	-636 ± 9	299 ± 7	149 ± 10
(3,6)	classical rotation (PIMC)	$(2.40 \pm 0.25) \times 10^4$	-898 ± 6	270 ± 7	
(3,6)	aligned molecule (DIAG)	2.44×10^4	-914 ± 1	270 ± 1	
(2,8)	quantum (DIAG)	50.6	-1234 ± 1	119 ± 1	3.9 ± 0.1
(2,8)	quantum (PIMC)	48.6 ± 2.5	-1235 ± 2	118 ± 3	-1.7 ± 16
(2,8)	classical rotation (PIMC)	21.4 ± 0.9	-1274 ± 3	104 ± 5	
(2,8)	aligned molecule (DIAG)	17	-1290 ± 1	99 ± 1	
(6,6)	quantum (DIAG)	2.5	-998 ± 1	47.1 ± 0.1	0.7 ± 0.1
(6,6)	quantum (PIMC)	2.5 ± 0.1	-998.7 ± 1.3	44 ± 6	-4 ± 9
(6,6)	classical rotation (PIMC)	2.4 ± 0.2	-1000.5 ± 1.2	46 ± 7	
(6,6)	aligned molecule (DIAG)	2.3	-1005 ± 1	42 ± 1	

[a]DIAG: direct diagonalization of the single-particle Hamiltonian. PIMC: path integral simulations. The "classical rotation" model treats the rotational degrees of freedom classically, but the translational degrees of freedom quantally. The "aligned molecule" results were obtained by assuming that a molecule is aligned with the nanotube axis and that rotations do not contribute to the selectivity. Acronyms as in Table 1.

Zero-Pressure Selectivity. The influence of the quantization of the rotational degrees of freedom on the selectivity is shown in Table 2, where we report zero-pressure *para*-T_2/*para*-H_2 selectivities and the average energies for *para*-H_2 confined in the various SWNTs according to different calculation methods. We report the results of PIMC simulations in two cases: the first is the full quantum treatment of the rotors, whereas in the second set of calculations, we have treated rotations as classical degrees of freedom. These results are compared with those obtained by direct diagonalization of the single-molecule Hamiltonian, as well as the case in which the molecules are considered to be perfectly aligned with the nanotube axis. Under conditions of strong confinement, this last case is expected to be comparable with the classical treatment of the rotational degrees of freedom.[9]

The calculations of the selectivity using the PIMC technique were performed using the identity transformation method described in eq 29. It is apparent that the explicit inclusion of the quantized rotational degrees of freedom has a dramatic effect on the selectivity in the narrowest (3,6) tube, where the selectivity jumps from 2.4×10^4 to 1.7×10^8, an increase larger than 7000-fold. In the other tubes, the increase in selectivity ascribed to the rotational degrees of freedom is much less dramatic, being on the order of 2.3 in the (2,8) tube and essentially negligible in the case of the (6,6) tube.

The physical origin of the contribution to the overall selectivity due to the quantization of the rotational degrees of freedom can be seen by analyzing the difference between the simulations in which the rotations are treated classically and those in which the rotations are treated quantally.

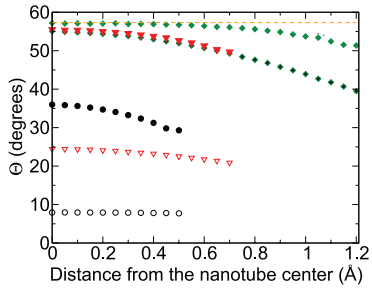

Figure 1. Average angle $\Theta = \langle \mathrm{acos}(|e_z|) \rangle$ between the nanotube and the molecular axes as a function of the distance from the nanotube center for H_2. Filled symbols: full quantum simulations. Open symbols: classical treatment of the rotational degrees of freedom. Circles refer to the (3,6) tube, triangles to the (2,8) tube, and diamonds to the (6,6) tube. The horizontal dashed line represents the value $\Theta_0 = 57.3°$, which corresponds to a random orientation.

In the presence of narrow confining potentials, one expects to find the molecules aligned with the nanotube axis, when rotations are treated classically. We have calculated the average angle $\Theta = \langle \mathrm{acos}(|e_z|) \rangle$ between the molecular axis of a single bead and the nanotube axis in the case of classical rotational degrees of freedom (and quantized translational ones) as a function of the distance of the molecule from the nanotube axis. The results are reported in Figure 1.

In the case when the rotations are treated classically, one can see that the value $\Theta \simeq 8°$ is obtained for molecules adsorbed in the (3,6) tube, thus confirming an almost perfect alignment with the nanotube axis. As the nanotube radius is increased, the angle tends to the value $\Theta_0 = 1$ rad $= 57.3°$, corresponding to a random orientation of the linear rotor. We notice that the angle tends to decrease for molecules away from the nanotube center. This phenomenon is due to the effect of the tube walls, whose repulsive potential favors molecular alignment.

The situation changes dramatically upon quantization of the rotational degrees of freedom because the confining effect of the potential energy is now counterbalanced by the quantum delocalization of the rotational degrees of freedom. The average angle Θ between the direction of the rotor corresponding to a given bead and the nanotube axis increases from 8 to about 35° in the case of the (3,6) and from 24 to 56° in the case of the (2,8) tube. The effect is much less pronounced for molecules confined in the (6,6) tube, where the calculations with classical or quantized degrees of freedom gave results almost consistent with free rotation.

Alternatively, the effect of quantum fluctuations on the orientation can also be seen by the high value of the rotational kinetic energy reported in Table 2. Hydrogen molecules confined in the narrowest tube have an average rotational kinetic energy of 147 K, which can be compared to the free-rotor rotational energy at the same temperature, which is on the order of 10^{-9} K due to the low probability of occupation of the first excited rotational state at that temperature. Due to the confining potential that tends to localize the molecular direction along the nanotube axis, the rotational ground state of the adsorbed rotor is a superposition of higher angular momentum states, resulting in a nonzero value of the average kinetic energy.

The net effect of the quantum rotational delocalization on the selectivity in narrow SWNTs can be appreciated in a semiclassical picture. If we consider a molecule at a given distance from the tube axis, then the quantization of the rotational degrees of freedom and the consequent rotational delocalization has the effect that the molecule sample regions with the potential energy is higher with respect to an almost perfectly aligned (classical) configuration. Therefore, the average potential acting on the center of mass is steeper when rotations are quantized than in the case when rotations are treated classically. Furthermore, the steepness is larger for the lighter molecule than for the heavier one. As a consequence, the adsorbed single-particle energy levels of the lighter rotors have a larger separation than the energy levels of the heavier species, not only because of the difference in mass but also because the quantization of rotations has a different effect on the two kinds of molecules.

Therefore, the net effect of quantized rotations is to enhance the spacing between the energy levels with a greater effect on the light isotope. In light of eq 2, this is reflected in a corresponding increase of the overall selectivity, as it is indeed observed in the simulations. By a careful analysis of numerically exact eigenstates of hydrogen isotopes confined in carbon nanotubes, Lu *et al.*[8] found that very high selectivities can be achieved in geometries so narrow that the ground state takes contributions from rotational states with finite angular momentum. We have been able to show,[9] using an approximate model for the description of the coupled rotational and translational degrees of freedom, that under these circumstances a very large contribution to the selectivity does indeed come from the rotational degrees of freedom, as is apparent in the exact result that we show in Table 2 for the (3,6) tube.

In the larger tubes, the average rotational kinetic energy is much smaller, indicating that the hydrogen isotopes are almost freely rotating, and the contribution of the rotational degrees of freedom to the selectivity is therefore smaller. In fact, one can still observe an enhancement of a factor of 2.3 in the (2,8) tube when quantized rotations are included, whereas in the (6,6) tube, quantized rotations do not significantly alter the results obtained assuming classical rotations.

Adsorption Isotherms. We have calculated the adsorption isotherms for different hydrogen isotopes in the (2,8) and (3,6) SWNTs using the BB grand canonical PIMC method for both the translational and rotational degrees of freedom. The results are shown in Figure 2

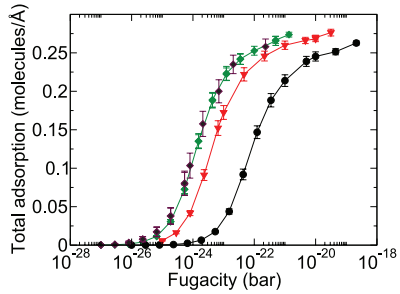

Figure 2. Pure fluid adsorption isotherms for hydrogen isotopes in the (2,8) carbon nanotube at $T = 20$ K. Circles, triangles, and diamonds refer to *para*-H_2, *ortho*-D_2, and *para*-T_2, respectively. Filled symbols represent simulations performed using the Boltzmann bias method, whereas open symbols represent the results obtained with the standard GCMC prescription. Lines are drawn as a guide for the eye.

for the case of the (2,8) tube and in Figure 3 for the case of the (3,6) tube.

We also report in Figure 2 the adsorption isotherm of *para*-T_2 in the (2,8) tube obtained with the standard path integral GCMC method.[32] This isotherm agrees very well with that obtained using the BB method, as it should, thus validating our implementation.

Quantum effects are quite sizable in the (2,8) SWNT, although not as dramatic as in the (3,6) nanotube, discussed below. The isotherms of the lightest and heaviest species are separated by about 2 orders of magnitude in pressure, as can be seen in Figure 2. As a general trend, note that the heavier species exhibits the highest adsorption at a given pressure. Qualitatively, one can think that the larger thermal de Broglie wavelength of the lighter species results in a larger effective Lennard-Jones radius, thus making adsorption in very narrow SWNTs less favorable.

This is apparent when considering adsorption in the (3,6) tube, reported in Figure 3. In this case, the uptake of T_2 begins to be appreciable at about 10^{-13} bar, whereas the adsorption of H_2 is essentially 0 below 10^{-5} bar. These two isotherms are separated by almost 8 orders of magnitude in pressure.

The quantum delocalization of the rotational degrees of freedom profoundly affects adsorption at high

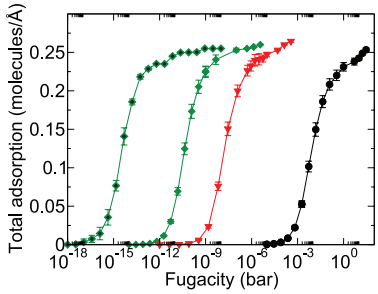

Figure 3. Pure fluid adsorption isotherms for hydrogen isotopes in the (3,6) carbon nanotube at $T = 20$ K. Circles, triangles, and diamonds refer to *para*-H_2, *ortho*-D_2, and *para*-T_2, respectively. The isotherm reported with empty diamonds corresponds to the case in which the rotational degrees of freedom are treated classically. Lines are drawn as a guide for the eye.

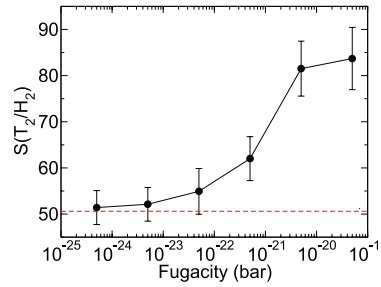

Figure 4. Finite pressure T_2/H_2 selectivity in the (2,8) tube at 20 K, using a bulk mole fraction of T_2 equal to $y_{T_2} = 0.1$. The horizontal line denotes the zero-pressure value (see Table 2), and circles are from path integral simulations. Lines are drawn as a guide to the eye.

coverages in much the same way as shown for the zero-coverage case discussed above. To investigate the magnitude of this effect at high loadings, we have treated the rotational degrees of freedom of T_2 classically and computed its adsorption in the (3,6) tube. These data are also plotted in Figure 3. This semiclassical isotherm is displaced to lower pressures by almost 4 orders of magnitude from the full quantum case.

Selectivity at Finite Pressures. In this section, we present path integral calculations for selectivities at finite pressures, up to loadings close to saturation for hydrogen isotopes in SWNTs. We have used the efficient identity transformation method of eq 32 to calculate the selectivity directly from its definition in eq 1.

The selectivities at finite pressures depend on the mole fraction of gases in the bulk. In contrast, the zero-pressure selectivities are independent of the bulk phase compositions. Simulation statistics for selectivity calculations will be better if the composition of the adsorbed phase is roughly equimolar, and therefore, we fixed the bulk mole fractions so that the adsorbed phase can be expected to have an approximately equimolar composition. Specifically, for given zero-pressure selectivity $S_0(A/B)$, bulk mole fractions such that $y_A/y_B \simeq 1/S_0$ should result in an almost 1:1 ratio in the adsorbed phase. We have therefore performed selectivity calculations in the (2,8) tube using a mole fraction $y_{T_2} = 0.1$ and calculations in the (3,6) tube using a mole fraction $y_{T_2} = 10^{-8}$.

The results of the calculations, shown in Figure 4 for the case of the (2,8) tube, show an increase of the selectivity with increasing pressure and predict a plateau in selectivity upon reaching saturation. A similar behavior is observed for the selectivity in the narrow (3,6) tube, as reported in Figure 5.

The reason for this behavior can be traced back to the structure of the adsorbed phase. Each of the two pure species occupies the same nanotube with an almost equal linear density of around 0.27 molecules/Å (recall that gases are adsorbed in single file in these narrow SWNTs). Therefore, one might expect an "average distance" $L \simeq 3.7$ Å between the molecules in the case of a saturated mixture. In going from zero to finite pres-

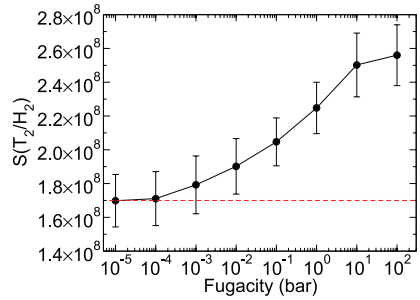

Figure 5. Finite pressure T_2/H_2 selectivity in the (3,6) tube at 20 K, using a bulk mole fraction of T_2 equal to $y_{T_2} = 10^{-8}$. The horizontal line denotes the zero-pressure value (see Table 2), and circles are from path integral simulations. Lines are drawn as a guide to the eye.

sures, one can then expect that the motion along the *z* coordinate of a given molecule is progressively hindered by the presence of the others, until a saturation condition is reached, and further compression of the system becomes more difficult.

This picture is validated by the results reported in Figure 6, where we plot the average center of mass kinetic energies for H_2 and T_2 as well as the average fluid−fluid energy for the mixture adsorbed in the (3,6) tube. We note that the average fluid−fluid potential energy per molecule tends to a constant value of $V \simeq -10$ K, indicating that the molecular configuration does not change very much after the onset of saturation.

The effect of the localization along the *z* direction is apparent from the behavior of the kinetic energies as a function of the loading. The values for T_2 and H_2, reported in Figure 6, do indeed show an increase at finite loading with respect to the zero-pressure value. This indicates a progressive hindrance of the motion along the nanotube axis, until the saturation point is reached and the kinetic energy tends to a constant value.

It is possible to make an estimate of these effects by assuming that—at saturation—all the molecules in the tube are separated from their neighbors by the same distance, L_{min}. In order to calculate L_{min}, one can assume that the molecules are placed single-file, with the molecular axis aligned with the nanotube. It is then

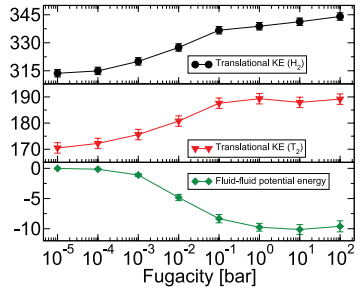

Figure 6. Average translational kinetic energy (circles, H_2; triangles, T_2) and average fluid−fluid potential energy (diamonds) for the adsorption of a T_2/H_2 mixture ($y_{T_2} = 10^{-8}$) in the (3,6) carbon nanotube at 20 K.

possible to calculate the average potential energy per particle, $V_{FF}(x)$, as a function of the distance *x* between the molecules, which is assumed to be the same for each pair of consecutive molecules.

The distance L_{min} is then calculated as the point of mechanical equilibrium, $\partial V_{FF}(x)/\partial x = 0$, obtaining the value $L_{min} = 3.74$ Å, which is close to the value computed from simulations of 3.7 Å. In this configuration, the potential energy per particle is $V_{FF}(L_{min}) = -39.3$ K.

We further assume that each of the isotopes performs harmonic motions around this mean-field potential energy minimum. In the actual system, of course, the dynamics is determined by anharmonic effects, so that the following estimate has only a heuristic value. The "spring constant" for these oscillation is evaluated to be $k_{HO} = \partial^2 V_{FF}/\partial x^2(L_{min}) = 281.3$ K/Å^2. Hydrogen isotopes oscillating in this harmonic potential would have a zero-point energy of $E_0^{H_2} = \hbar(k_{HO}/m_{H_2})^{1/2}/2 = 41.3$ K and $E_0^{T_2} = 23.8$ K for H_2 and T_2, respectively. The gain in kinetic energy measured from simulation (Figure 6) at high loadings due to the motion along tube axis is $\Delta E_{kin}^{H_2} \simeq 30$ K and $\Delta E_{kin}^{T_2} \simeq 19$ K for H_2 and T_2, respectively.

The average fluid−fluid potential energy, in the case of equimolar composition, should be on the order of $\Delta V = (2V_{FF}(L_{min}) + \Delta E_{kin}^{H_2} + \Delta E_{kin}^{T_2})/2 \simeq -7$ K. This is in good agreement with the value computed from simulation of $V_{FF} = -9.6 \pm 0.9$ K.

One can further estimate the asymptotic value of the selectivity at finite pressure by assuming the that its value at saturation is given by the product of the zero-pressure value S_0 and the selectivity S_{HO} due to the effective 1D harmonic oscillator discussed above. Using an independent particle approach,[2,3] the value of S_{HO} corresponding to T_2 and H_2 in a harmonic oscillator of spring constant k_{HO} turns out to be $S_{HO} = 1.5$, in reasonable agreement with the observed behavior of the selectivity (see Figure 4 and Figure 5).

CONCLUSIONS

In this paper, we presented numerical results for the calculation of the *para*-T_2/*para*-H_2 selectivity in various carbon nanotubes at 20 K. We have discussed, in particular, the effect of the quantized rotational degrees of freedom on the selectivity by developing a simulation method that allows a classical treatment of the rotations while keeping a quantum treatment of the translational degrees of freedom.

We showed that the explicit inclusion of quantized rotations enhances the zero-pressure selectivity by a factor of more than 7000 in the (3,6) nanotube, which is the narrowest tube we have investigated. Rotational effects are essentially negligible for the (6,6) SWNT. The rotational degrees of freedom contribute less than a factor of 2 in the (2,8) SWNT at zero pressure.

We investigated the effect of finite pressures on the adsorption and the selectivity, extending the BB

method to the case of rigid rotors. We calculated the adsorption isotherms of various hydrogen isotopes in different tubes at 20 K and showed that quantum effects hinder the adsorption of the lighter species, whose isotherm turns out to be separated by many orders of magnitude in pressure from that of the heavier species.

We calculated the pressure dependence of the selectivity and found that for a bulk H_2/T_2 mixture the selectivity in narrow SWNTs increases form its zero-pressure value when the loading in the nanotube approaches saturation. This behavior has been correlated to the confinement of the molecular motion along the nanotube axis. At high loadings in very narrow nanotubes, there is a transition from 2D to 3D confinement.

In order to perfom these calculations, we developed novel algorithms for the hybrid path integral Monte Carlo simulation of rigid diatomic molecules accounting for both quantum translation and rotation, showing how to calculate the torques from the expression of the rotational density matrix. In order to efficiently sample a collection of quantized rotors, we have also developed a velocity Verlet-like integrator based on a multiple timestep approach.

We would like to point out that this methodology can find application in studying hydrogen under any kind of confinement. For example, one might use it to simulate the recently characterized states of hydrogen confined into fullerene cages.[33−35]

METHODS

Selectivity. The adsorption selectivity of two hydrogen isotopes *A* and *B*, say T_2 and H_2, is defined as:

$$S(A/B) = \frac{x_A/x_B}{y_A/y_B} \tag{1}$$

where *x* and *y* are the mole fractions in the adsorbed and bulk phases, respectively. An important simplification of eq 1 can be obtained in the limit of zero pressure when one can neglect the adsorbate−adsorbate interaction. It can be shown that in this case the selectivity depends only on the energy levels $E^{(l)}$ of the adsorbed molecules, and can be written as[4,5]

$$S_0(A/B) = \frac{Q_B^{\text{free}}}{Q_A^{\text{free}}}\frac{Q_A}{Q_B} = \left(\frac{m_B}{m_A}\right)^{d/2}\frac{Q_B^{\text{free-rot}}}{Q_A^{\text{free-rot}}}\left[\frac{\sum_l \exp(-E_A^{(l)}/k_BT)}{\sum_l \exp(-E_B^{(l)}/k_BT)}\right] \tag{2}$$

where Q^{free} is the molecular partition function for the ideal gas, $Q^{\text{free-rot}}$ is the free-rotor molecular partition function, and *Q* is the molecular partition function for the given species. We have denoted by *d* the number of spatial dimensions in which confinement takes place. In the case of hydrogen molecules in carbon nanotubes, $d = 2$. In the zero-pressure limit, the selectivity is a function of the energy levels of the two species, which can be obtained by a direct diagonalization of the single-particle Hamiltonian.

In the general case, the calculation of the selectivity of an *A*/*B* mixture can be performed by a direct calculation of the mole fractions appearing in the definition given in eq 1. In this case, grand canonical Monte Carlo simulations have been shown to be particularly effective.[4,10] However, direct calculation is not efficient under conditions of strong confinement,[8,9] which is the regime of interest of this work. We have therefore developed novel methods to efficiently sample path integral configurations of adsorbed hydrogen isotopes subject to extreme confinement.

Diagonalization of the Single-Particle Hamiltonian. The Hamiltonian $\hat{H}$ of a collection of *N* rigid rotors in an external potential is given by

$$\hat{H} = \sum_{i=1}^{N} -\frac{\hbar^2}{2M}\nabla_i^2 + \sum_{i=1}^{N}\frac{\hat{L}_i^2}{2I} + \sum_{i<j} v(\hat{x}_i\hat{\Omega}_i;\hat{x}_j\hat{\Omega}_j) + \sum_{i=1}^{N} v_{\text{ext}}(\hat{x}_i\hat{\Omega}_i) \tag{3}$$

and is a function of the mass *M*, the angular momentum $\hat{L}$, and the moment of inertia *I* of the molecules. We have introduced a fluid−fluid pair interaction potential *v* and a solid−fluid interaction potential v_{ext}. The quantities $\hat{x}_i$ and $\hat{\Omega}_i$ denote the operators for the center of mass position and the orientation of molecule *i*, respectively. The Hamiltonian is the sum of the translational (center of mass) kinetic energy $\hat{T}$, the rotational kinetic energy $\hat{K}$, the fluid−fluid potential energy $\hat{V}$, and the solid−fluid potential energy $\hat{V}_{\text{ext}}$.

In the limit of zero coverage, the fluid−fluid interaction potential in eq 3 can be neglected and the Hamiltonian becomes the sum of single-particle contribution, which can be straightforwardly diagonalized. The single-particle energy levels can be used to estimate the zero-pressure selectivity using eq 2.

We performed a direct diagonalization of the single-molecule quantum Hamiltonian in the case of H_2 and T_2 adsorbed in the (3,6), (2,8), and (6,6) SWNTs, using the interaction potential specified below. We used as basis set functions of the form

$$\Psi_{MNlm}(r, \alpha, z;\theta, \phi) \propto J_N(k_M r)e^{iM\alpha}Y_{lm}(\theta, \phi)e^{ikz} \tag{4}$$

where $Y_{lm}(\theta, \phi)$ are the eigenfunctions for a free rigid rotor, *r* and α are polar coordinates in a plane orthogonal to the nanotube axis and $J_N(k_M r)$ is a Bessel function, where k_M is chosen so that J_N is a radial eigenstate for a free particle confined in a rigid cylinder of radius *R*. The value of the parameter *R* has been chosen so that the solid−fluid interaction $v_{\text{ext}}(R, \Omega)/k_B$ is at least 10^4 K irrespective of the orientation Ω of the rotor. We have checked that this choice does not appreciably affect the results obtained.

We reached convergence in the calculation of the selected properties by using 117 translational functions and 45 rotational states in the case of the (3,6) tube, 181 translational functions and 15 rotational states in the case of the (2,8) tube, and 240 translational functions together with 15 rotational states in the case of the (6,6) tube.

Path Integral Formulation of Statistical Mechanics. The quantum mechanical expression for the partition function of a system of *N* rigid linear rotors is

$$Q = \int \mathrm{d}^{3N}X_1\mathrm{d}^{2N}\Omega_1\langle X_1\Omega_1|\exp[-\beta\hat{H}]|X_1\Omega_1\rangle \tag{5}$$

where *X* denotes a vector with the 3*N* center of mass coordinates of the rotors, and Ω denotes the set of the 2*N* angles describing their orientations. A subscript 1 has been introduced for later convenience.

The quantum partition function of eq 5 can be rewritten by repeatedly applying the Trotter identity

$$\exp[A + B] = \lim_{P\to\infty}(\exp[A/P]\exp[B/P])^P \tag{6}$$

which is valid for generally noncommuting operators *A* and *B* and further approximated by assuming a large but finite Trotter number *P*, obtaining

$$Q \simeq \int \mathrm{d}^{3N}X_1\mathrm{d}^{2N}\Omega_1\langle X_1\Omega_1|\prod_{j=1}^{P}\exp(-\beta\hat{T}/P)\exp(-\beta\hat{K}/P)\exp[-\beta(\hat{V}+\hat{V}_{\mathrm{ext}})/P]|X_1\Omega_1\rangle \quad (7)$$

We can now introduce $P-1$ completeness relations of the form

$$\mathbf{1} = \int \mathrm{d}^{3N}X_i\mathrm{d}^{2N}\Omega_i|X_i\Omega_i\rangle\langle X_i\Omega_i| \quad (8)$$

between the factors in eq 7 and write the partition function as

$$\begin{aligned} Q \simeq & \int \mathrm{d}^{3N}X_1\mathrm{d}^{2N}\Omega_1\ldots\mathrm{d}^{3N}X_P\mathrm{d}^{2N}\Omega_P \\ & \langle X_1\Omega_1|\exp(-\beta\hat{T}/P)\exp(-\beta\hat{K}/P)\exp[-\beta(\hat{V}+\hat{V}_{\mathrm{ext}})/P]|X_2\Omega_2\rangle \\ & \langle X_2\Omega_2|\exp(-\beta\hat{T}/P)\exp(-\beta\hat{K}/P)\exp[-\beta(\hat{V}+\hat{V}_{\mathrm{ext}})/P]|X_3\Omega_3\rangle \\ & \ldots \\ & \langle X_P\Omega_P|\exp(-\beta\hat{T}/P)\exp(-\beta\hat{K}/P)\exp[-\beta(\hat{V}+\hat{V}_{\mathrm{ext}})/P]|X_1\Omega_1\rangle \\ = & \int \mathrm{d}^{3N}X_1\mathrm{d}^{2N}\Omega_1\ldots\mathrm{d}^{3N}X_P\mathrm{d}^{2N}\Omega_P\times \\ & \prod_{i=1}^{P}\langle X_i\Omega_i|\exp(-\beta\hat{T}/P)\exp(-\beta\hat{K}/P)\exp[-\beta(\hat{V}+\hat{V}_{\mathrm{ext}})/P]|X_{i+1}\Omega_{i+1}\rangle \end{aligned} \quad (9)$$

where we have used the identities $X_{P+1} = X_1$ and $\Omega_{P+1} = \Omega_1$. The set of coordinates X_i will be said to identify the ith slice. Each of the matrix elements appearing in the previous equation can be written as

$$\begin{aligned} \langle X_i\Omega_i|\exp(-\beta\hat{T}/P)\exp(-\beta\hat{K}/P)\exp[-\beta(\hat{V}+\hat{V}_{\mathrm{ext}})/P]|X_{i+1}\Omega_{i+1}\rangle = \\ \langle X_i|\exp(-\beta\hat{T}/P)|X_{i+1}\rangle\langle\Omega_i|\exp(-\beta\hat{K}/P)|\Omega_{i+1}\rangle\exp[-\beta(V(X_{i+1}\Omega_{i+1}) + V_{\mathrm{ext}}(X_{i+1}\Omega_{i+1}))/P] \end{aligned} \quad (10)$$

A straightforward calculation shows that the expectation value of the translational kinetic energy Boltzmann factor assumes the form[36]

$$\langle X_i|\exp(-\beta\hat{T}/P)|X_{i+1}\rangle = a\exp(-\beta\kappa|X_i - X_{i+1}|^2/2) \quad (11)$$

where the amplitude a and the spring constant κ are given by

$$a = \left(\frac{Mk_{\mathrm{B}}TP}{2\pi\hbar^2}\right)^{3/2} \quad (12)$$

$$\kappa = \frac{MP(k_{\mathrm{B}}T)^2}{\hbar^2} \quad (13)$$

and the expectation value of the rotational kinetic energy Boltzmann factor becomes[37]

$$\begin{aligned} & \langle\Omega_i|\exp(-\beta\hat{K}/P)|\Omega_{i+1}\rangle = \\ & \sum_{n=1}^{N}\sum_{J=0}^{\infty}\frac{2J+1}{4\pi}P_J(\cos\theta_{i,i+1}^{n})\exp[-\beta J(J+1)B/P] \\ & \equiv \sum_{n=1}^{N}\Xi(\theta_{i,i+1}^{n}) \end{aligned} \quad (14)$$

where $P_J(\cdot)$ is a Legendre polynomial and $\theta_{i,i+1}^{n}$ is the angle between the directions Ω_i and Ω_{i+1} of molecule n in two adjacent slices i and $i+1$. $B = \hbar^2/(2I)$ is the rotational constant of the rotor and the last equation defines the quantity Ξ.

In the case of homonuclear molecules, the indistinguishability of the nuclei imposes some restrictions on the sum in eq 14 according to the spin states of the nuclei. For *para*-H_2, *ortho*-D_2, and *para*-T_2, as in this work, the summation on the angular momenta J in eq 14 is limited to the even numbers only[37] and results in a positive definite density matrix, which can be directly used in the Monte Carlo simulations.

For *ortho*-H_2, *ortho*-T_2, and *para*-D_2 rotational states, the sum is restricted to the odd angular momentum states, resulting in a density matrix that is not positive definite. As a consequence, more care has to be taken in performing a Monte Carlo simulation in this case.[37,38]

The net effect of these algebraic manipulations is that we have been able to rewrite the original quantum partition function of an N particle system (eq 5) as a classical partition function of a NP particle system. The NP particles of the classical equivalent are naturally divided into P slices of N particles each. Each particle in a slice interacts with all the other particles in the same slice *via* the original intermolecular and intramolecular potential divided by a factor of P (see eq 10). Quantum mechanical effects are taken into account by the interaction of each particle with the corresponding copy on the previous and following slice; the center of mass coordinates are bound by the harmonic potential of eq 11, and the orientations give rise to the interslice rotational partition function of eq 14. The resulting system is then equivalent to a classical collection of N ring polymers, each having P beads. A rigid linear rotor of inertia moment I is associated with each of these beads. The ith bead on a given polymer interacts only with the corresponding bead on the other polymers *via* the original intermolecular potential (rescaled by a factor of P). The interaction between the beads of a given ring polymer is described by a harmonic interaction on the translational coordinates with the two adjacent beads (see eq 11) and an interaction between the orientational degrees of freedom of adjacent beads whose density matrix is given by eq 14.

Hybrid Monte Carlo Method. Given the quantum to classical mapping described in the previous section, it follows that classical Monte Carlo methods can be used to calculate quantum thermodynamic properties. Since we expect to work under conditions where quantum mechanics is not a small correction, it will be necessary to use large values of the Trotter number P. In this case, the simple Metropolis method for sampling of the translational and rotational phase space, such as that discussed by Cui *et al.*,[39] will be affected by slow convergence due to the different magnitudes of the intramolecular potential and quantum spring potential at high Trotter numbers, which scale as $1/P$ and P, respectively.

In this work, we use the HMC method,[40,41] which consists of choosing a new candidate configuration by performing a molecular dynamics (MD) move with a large time step; the resulting configuration is then accepted or rejected using a standard Metropolis condition on the difference in the *total* energy (which is not conserved if a large enough time step is taken). The difference in magnitude of the intramolecular and quantum spring potentials described above can be naturally overcome in the MD framework by devising a multiple timestep procedure,[42] described in detail below.

In order to perform an MD move, one has to know the forces and the torques acting on each of the rotors. The potential energy between the molecules on the same slice is given by the rescaled original potential, and the quantum mechanical effects on the translational degrees of freedom are described by a simple harmonic potential between adjacent slices (see eq 11). The only unknown is the quantum torque between the molecules in adjacent slices; we calculate the torque numerically, starting from the expression of the density matrix in eq 14. Since eq 14 takes the form of a Boltzmann factor, it can generally be written as $\langle\Omega_i|\exp(-\beta\hat{K}/P)|\Omega_{i+1}\rangle = C\exp[-\beta U_{\mathrm{rot}}(\theta)]$, where C is an unknown constant and $U_{\mathrm{rot}}(\theta)$ is the quantum rotational potential energy between two rotors in adjacent slices, whose orientations form an angle θ with one another.

We note in passing that for heteronuclear molecules in the limit $PT \gg 1$, U_{rot} is given to a good approximation by the harmonic expression $U_{\mathrm{rot}}(\theta) = K\theta^2/2$ with K given by[38]

$$K = \frac{IP(k_{\mathrm{B}}T)^2}{\hbar^2} \quad (15)$$

similar to the analogous expression for the translational coordinates, eq 13.

In general, the modulus of the quantum torque can be written as

$$N_{quant}(\theta) = -\frac{dU_{rot}(\theta)}{d\theta} = \frac{k_B T}{\Xi} \sin\theta \frac{d\Xi(\theta)}{d\cos\theta} \quad (16)$$

The direction of the torque is obviously orthogonal to the plane generated by the two orientations of the interacting molecules, and it tends to close the angle between the two molecules. The derivative in eq 16 can be evaluated either numerically or using the identity

$$\frac{dP_l(x)}{dx} = \frac{lxP_l(x) - lP_{l-1}(x)}{x^2 - 1} \quad (17)$$

Multiple Timestep Algorithm. Inspection of eqs 10, 13, and 15 shows that the intermolecular forces scale like the inverse of the Trotter number P, whereas the quantum forces (and, possibly, the torques) are proportional to it. In order to efficiently sample phase space using an HMC method, it is necessary that all of the degrees of freedom contribute uniformly to the nonconservation of energy when a MD timestep is performed.

To this end, we use a multiple timestep method to perform the MD evolution:[42] we divide the forces into "long-range" (the intermolecular forces, in our case) and "short-range" (the quantum forces and torques). We integrate the long-range forces using a timestep Δt, which is divided into smaller timesteps where only the short-range forces are evaluated as the system is propagated.

In our case, we do not know the typical time scale of the quantum rotation, so we have decided to use three nested loops: we use a long timestep Δt to propagate the system according to the intermolecular forces, an intermediate timestep δt to propagate the rotational degrees of freedom, and an inner timestep $\delta\tau$ to propagate the quantum spring forces on the translational degrees of freedom.

We also need a reversible algorithm to integrate all of the degrees of freedom in order for the hybrid method to work. It is well-known that the velocity form of the Verlet algorithm is reversible and can be used in multiple timestep methods.[42] Instead of using algorithms already developed to treat the general motion of rigid rotors in a multiple timestep framework,[43,44] we have developed a velocity Verlet-like integrator for the rotational motion of a rigid linear rotor that can be easily coupled to the velocity Verlet evolution of the center of mass coordinates. Details of its derivation are given below.

Denoting by x and v the translational positions and velocities, and by e and ϖ the direction of the molecular axes and the molecular angular velocities, the multiple timestep method is implemented as follows:

Calculate F_{long} and N_{long} (intermolecular forces)

$$v \rightarrow v + \Delta t F_{long}/(2M)$$

$$\varpi \rightarrow \varpi + \Delta t N_{long}/(2I)$$

Loop over $\Delta t/\delta t$
Calculate N_{short} (quantum torque)

$$\varpi \rightarrow \varpi + \delta t N_{short}/(2I)$$

Loop over $\delta t/\delta\tau$
Calculate F_{short} (quantum spring)

$$v \rightarrow v + \delta\tau F_{short}/(2M)$$

$$e \rightarrow e + \delta\tau\varpi \times e - (\delta\tau)^2\varpi^2/2$$

normalize e

$$x \rightarrow x + v\delta\tau$$

Calculate F_{short}

$$v \rightarrow v + \delta\tau F_{short}/(2M)$$

Calculate N_{short}

$$\varpi \rightarrow \varpi + \delta t N_{short}/(2I)$$

Calculate F_{long} and N_{long}

$$v \rightarrow v + \Delta t F_{long}/(2M)$$

$$\varpi \rightarrow \varpi + \Delta t N_{long}/(2I)$$

Calculate the final translational and rotational kinetic energies.

The algorithm presented above is based on the assumption that the fastest moving degrees of freedom are the internal translational degrees of freedom of the ring polymers, followed by the rotational motions of the rotors and, finally, by the overall (center-of-mass) translation of the ring polymers.

We have checked that this is indeed the case by calculating the Einstein frequencies $\omega_L^2 = \mathbf{F}_{long}^2/(Mk_BT)$ corresponding to the intermolecular forces, the quantum torques ($\omega_N^2 = \mathbf{N}_{short}^2/(Ik_BT)$) and the quantum spring forces ($\omega_S^2 = \mathbf{F}_{short}^2/(Mk_BT)$) in the various configurations under investigation. We have found that usually $\omega_S/\omega_N \simeq 2$, indicating that indeed the fastest motions correspond to the internal translational degrees of freedom of the ring polymers. We have therefore set the ratio $\delta t/\delta\tau = 2$.

On the other hand, the ratio $\Delta t/\delta t$ depends strongly on the isotope mass (which determines the stiffness of the spring joining the beads in the quantum-classical path integral isomorphism) and the extent of confinement to which the molecule is subjected (which is related to the stiffness of the nanotube−hydrogen interaction). We have chosen this ratio to be equal to ω_N/ω_L, with typical values ranging from 8 in the case of H_2 in the (3,6) tube to 45 in the case of T_2 in the (2,8) tube. When considering mixtures, we have set $\Delta t/\delta t$ to the largest of the values for the pure species.

The reliability of the algorithm has been checked by comparing its results to those obtained by direct diagonalization of an isolated rotor adsorbed within nanotubes of various sizes (see Table 1).

Velocity Verlet Integrator for Rigid Linear Molecules. The classical dynamics of a rigid rotor is described by the equations

$$\frac{d\mathbf{e}}{dt} = \varpi \times \mathbf{e} \quad (18)$$

$$I\frac{d\varpi}{dt} = N \quad (19)$$

where $\mathbf{e}$ is a unit vector in the direction of the rotor and, ϖ is the angular velocity, I is the moment of inertia, and N is the torque applied to the system.

These dynamical variables are redundant because the norm of the vector $\mathbf{e}$ is a constant of the motion described by the previous equations. Since the torque N is, by construction, always orthogonal to the axis vector, the component of the angular velocity along the unit vector is also a constant of motion. Since the moment of inertia of a linear rotor with respect to the symmetry axis is 0, the component of the angular velocity along this axis is also 0.

The previous equations cannot be put in the form of a Hamiltonian system. In order to develop a time-reversible integrator that can be used in the HMC method, we demonstrate that it is indeed possible to integrate the equations using a velocity Verlet-like integrator, adapted to take into account the above constraint. A multiple timestep algorithm can then be developed by analogy to the velocity Verlet case.

Using the Taylor expansion we can write

$$\mathbf{e}(t + \delta t) \simeq \mathbf{e}(t) + \delta t\frac{d\mathbf{e}(t)}{dt} + \frac{1}{2}(\delta t)^2\frac{d^2\mathbf{e}(t)}{dt^2} \quad (20)$$

$$= \mathbf{e} + \delta t(\varpi \times \mathbf{e}) + \frac{1}{2}(\delta t)^2\frac{d}{dt}(\varpi \times \mathbf{e}) \quad (21)$$

$$= \mathbf{e} + \delta t(\varpi \times \mathbf{e}) + \frac{1}{2}(\delta t)^2\left(\frac{d\varpi}{dt} \times \mathbf{e} + \varpi \times (\varpi \times \mathbf{e})\right) \quad (22)$$

$$= \mathbf{e}(t) + \delta t\left[\left(\varpi(t) + \frac{\delta t}{2}\frac{N(t)}{I}\right) \times \mathbf{e}(t)\right] - \frac{(\delta t)^2}{2}\varpi^2(t)\mathbf{e}(t) \tag{23}$$

where we have restored the explicit time dependence in the last equation.

The last term in eq 23 assures that the length of the unit vector describing the direction of the rotor remains fixed. In our code, we renormalize the unit vector after each time step.

The equation for the angular velocity becomes

$$\varpi(t + \delta t) \simeq \varpi(t) + \delta t\frac{d\varpi(t)}{dt} + \frac{(\delta t)^2}{2}\frac{d^2\varpi(t)}{dt^2} \tag{24}$$

$$= \varpi + \frac{\delta t}{2}\dot{\varpi} + \frac{\delta t}{2}(\dot{\varpi} + \delta t\ddot{\varpi}) \tag{25}$$

$$= \varpi(t) + \frac{\delta t}{2}\frac{N(t)}{I} + \frac{\delta t}{2}\frac{N(t + \delta t)}{I} \tag{26}$$

So that one can construct a velocity Verlet-like algorithm for the rotational degrees of freedom as

1. Calculate the angular velocity at half timestep $\varpi(t + \delta t/2) = \varpi(t) + (\delta t/2)(N(t)/I)$
2. Advance the orientation **e** at full timestep, using eq 23
3. Calculate the torques at the time $t + \delta t$
4. Advance the angular velocity at full timestep

Classical Treatment of the Rotational Degrees of Freedom. In order to assess the importance of the quantized rotational degrees of freedom to the quantum selectivity, we now present a formalism to describe a system in which only the translational degrees of freedom are quantized and the rotations are described classically. In what follows, we perform the derivation referring to a single rotor in an external potential, in order to avoid cumbersome notation. The extension to interacting rotors is straightforward.

Consider a system whose Hamiltonian is given by $H = T(\hat{p}) + K(\hat{L}) + V(\hat{x}, \hat{\Omega})$, where $T(\hat{p}) = \hat{p}^2/2m$ is the kinetic energy of translation, $K(\hat{L}) = B\hat{L}^2$ is the kinetic energy of rotation and $V(\hat{x}, \hat{\Omega})$ is the potential energy with a dependence on the center of mass position operator $\hat{x}$ and the orientation operator $\hat{\Omega}$. The quantum mechanical partition function is given by

$$Q = \int dx \sum_{l,m} \langle x;l,m|\exp[-\beta(T + K + V)]|x;l,m\rangle \tag{27}$$

The classical treatment of some of the degrees of freedom correspond to the assumption that the operators of the corresponding generalized coordinates and momenta commute between them, as well as with all other relevant observables. Since we are interested in approximating the rotation as classical, we proceed as if the rotational kinetic energy and the potential, which depends on the molecular orientation, obey the commutation relation $[\hat{V}, \hat{K}] = 0$, which implies $\exp[-\beta(T + V + K)] = \exp[-\beta(T + V)]\exp[-\beta K]$. One can then perform the partial trace over the rotational degrees of freedom, obtaining

$$\begin{aligned}
\rho &= \mathrm{Tr}_{\mathrm{rot}}\exp[-\beta(T + K + V)] \\
&= \sum_{lm} \langle l,m|\exp[-\beta(T + K + V)]|l,m\rangle \\
&= \sum_{lm} \langle l,m|\exp[-\beta(T + V)]|l,m\rangle e^{-\beta Bl(l+1)} \\
&= \int d\Omega_1 d\Omega_2 \sum_{lm} \langle lm|\Omega_1\rangle\langle\Omega_1|\exp[-\beta(T + V)]|\Omega_2\rangle\langle\Omega_2|l,m\rangle e^{-\beta Bl(l+1)} \\
&= \int d\Omega_1 d\Omega_2 \sum_{lm} Y^*_{lm}(\Omega_1)Y_{lm}(\Omega_2)\langle\Omega_1|\Omega_2\rangle\exp[-\beta(T + V(x,\Omega_2))]e^{-\beta Bl(l+1)} \\
&= \int d\Omega_1 \left(\sum_l \frac{2l + 1}{4\pi} e^{-\beta Bl(l+1)}\right)\exp[-\beta(T + V(x,\Omega_1))] \\
&= Q_{\mathrm{rot}} \int \frac{d\Omega}{4\pi}\exp[-\beta(T(\hat{p}) + V(\hat{x},\Omega))]
\end{aligned} \tag{28}$$

where Q_{rot} is the molecular partition function of the free rotor. In the last expression, the orientation Ω is the classical orientation of the rotor and $\hat{p}$ and $\hat{x}$ are the momentum and position operators (still quantum mechanical).

When one applies the Trotter formula to the reduced density matrix ρ given by eq 28, each of the beads corresponding to a given molecule has the molecular axis pointing in the same direction as the others. Considering Ω as a classical variable is therefore equivalent to suppressing its fluctuation due to the Heisenberg uncertainty principle.

Path Integral Calculation of the Zero-Pressure Selectivity. In the framework of path integral Monte Carlo, the zero-pressure selectivity can be calculated by extending the identity transformation method developed by Challa *et al.*[3] for spherical molecules to rigid rotors. The zero-pressure selectivity can then be written as

$$S_0(A/B) = C\langle\exp[-\beta\Delta U_{B\to A}]\rangle_B \tag{29}$$

where

$$\Delta U_{B\to A} = \int_{m_B}^{m_A} dm\left(\frac{dU_{\mathrm{int}}}{dm}\right) \tag{30}$$

is the variation of the quantum potential energy when a molecule of type *B* is gradually transformed into a molecule of type *A* by performing a number N_{MC} of Monte Carlo steps. The constant *C* is given by

$$C = \frac{Q^{\text{free-rot}}(B)}{Q^{\text{free-rot}}(A)}\left(\frac{m_A}{m_B}\right)^{3/2(P-1)}\left(\frac{I_A}{I_B}\right)^P \tag{31}$$

where the average in eq 29 is performed on a simulation of the lightest species, *B*, only. The number points necessary to reach convergence in the evaluation of the integral in eq 30 for the *B* to *A* transformation is on the order of $N_{MC} = 5000$.

In performing the calculations, we used a system of at least 50 non-interacting molecules confined inside a carbon nanotube. We used at least 20000 HMC steps for equilibration, and a production run of at least 20 000 HMC. The selectivity was calculated from eq 29, with configurations sampled every 50 HMC steps.

Path Integral Calculation of Adsorption at Finite Pressure under Strong Confinement: The Boltzmann Bias Method. In order to calculate the selectivity at finite pressures, Challa *et al.*[4] have used straightforward grand canonical simulations of mixtures to obtain the mole fraction to insert in eq 1. In this case, a trial insertion move is performed by placing ring polymers in the nanotube with configurations drawn from an ideal gas distribution. The usual insertion and deletion moves are performed for the heavier species only (T_2 in our case), whereas the lighter species is inserted or deleted by performing $T_2 \leftrightarrow H_2$ transformations. A transformation move of a molecule of the species 1 into a molecule of the species 2 is accepted with the probability

$$P_{1\to 2} = \min\left[1, \frac{N_1}{N_2 + 1}\left(\frac{\Lambda_1}{\Lambda_2}\right)^3\exp[\beta(\mu_2 - \mu_1)]\exp[-\beta\Delta U^{\mathrm{ext}}]\right] \tag{32}$$

where N_i is the number of molecules of type *i* in the system before the transformation is attempted, Λ is the de Broglie wavelength, μ the chemical potential (which is different for the two species to account for a given bulk molar composition), and ΔU^{ext} is the difference of the sum of the fluid−fluid and solid−fluid potential energies between the configurations (N_1, N_2) and $(N_1 - 1, N_2 + 1)$. Note that, in order to fulfill the detailed balance condition, the probability of a $T_2 \to H_2$ transformation attempt must be equal to the probability of attempting the reverse move.

The method outlined above works with reasonable efficiency only when the ideal gas ring polymer configurations used in the insertion moves have a reasonable probability of being accepted, as it happens when trying to insert gas phase polymers into moderately large tubes. When adsorbed molecules are in the X2DC regime,[8] as it happens in the case of the (3,6)

tube, the acceptance ratio for insertion drops to very small values, less than one in a million attempts. As a consequence, equilibration is unacceptably slow and statistical accuracy is low. To overcome the limitations of the standard grand canonical algorithm, one of us has recently developed an efficient method to improve the acceptance ratio of insertion moves, termed Boltzmann bias grand canonical Monte Carlo.[10] Here we extend this procedure to the case of adsorption of quantized rigid rotors in highly confining geometries.

Using the detailed balance condition, the ratio between the transition probabilities for insertion, $W_{N\to N+1}$, and deletion, $W_{N+1\to N}$, in the path integral formalism can be written as

$$\frac{W_{N\to N+1}}{W_{N+1\to N}} = \frac{1}{N+1}\exp(\beta\mu - \beta\Delta U_{FF} - \beta\Delta U_{SF}) d^3X \prod_{i=1}^{P} \times \langle \Omega_i x_i | e^{-\beta(\hat{T}+\hat{K})/P} | \Omega_{i+1} x_{i+1} \rangle d\Delta_i d\Omega_i \qquad (33)$$

where μ is the chemical potential of the species to be inserted with one bead in position X. ΔU_{FF} and ΔU_{SF} are the fluid−fluid and solid−fluid potential energy of interaction of the particle inserted, $\hat{T}$ is the translational kinetic energy operator, and $\hat{K}$ is the rotational kinetic energy operator. One can further write

$$\prod_{i=1}^{P} \langle \Omega_i x_i | e^{-\beta(\hat{T}+\hat{K})/P} | \Omega_{i+1} x_{i+1} \rangle = \frac{1}{\Lambda^3} F(\Delta_1, ..., \Delta_{P-1}) \times q_{rot}\rho(\Omega_1, ..., \Omega_P) \qquad (34)$$

where $F(\Delta_1,..., \Delta_P)$ is the probability distribution for the distances $\Delta_i = x_{i+1} - x_i$ between the beads for polymers drawn from an ideal gas distribution[10] and $\rho(\Omega_1,..., \Omega_P)$ is the probability distribution for the relative orientations of the rotors associated with each bead in the ideal gas phase. We have denoted by q_{rot} the rotational partition function of a free rotor.

The transition probability $W_{N\to N+1}$ can be written as the product of an insertion probability $I_{N\to N+1}$ and an acceptance probability $A_{N\to N+1}$. The BB method is based on the choice

$$I_{N\to N+1} = \frac{1}{Q_{ads}} e^{-\beta U_{SF}} F(\Delta_1, ..., \Delta_{P-1}) q_{rot} \rho(\Omega_1, ..., \Omega_P) \frac{d^3X}{\Lambda^3} \prod_{i=1}^{P} d\Delta_i d\Omega_i \qquad (35)$$

for the insertion probability, where

$$Q_{ads} = \int e^{-\beta U_{SF}} F(\Delta_1, ..., \Delta_{P-1}) q_{rot} \rho(\Omega_1, ..., \Omega_P) \frac{d^3X}{\Lambda^3} \prod_{i=1}^{P} d\Delta_i d\Omega_i \equiv \exp(-\beta\tilde{\mu}) \qquad (36)$$

and the last equality defines the quantity $\tilde{\mu}$. By "undoing" the Trotter factorization in eq 36, it can be shown that Q_{ads} is the partition function of a single quantum rotor moving in the external potential U_{SF}. In the following, $\tilde{\mu}$ has been calculated from the knowledge of the energy levels of isolated adsorbed rotors, obtained by diagonalizing the Hamiltonian of rotors confined in nanotubes with a method described above. Notice that under conditions of strong confinement—when the difference between the ground state and the first excited level exceeds k_BT—the quantity $\tilde{\mu}$ defined above tends to the energy of the ground state of an isolated adsorbed rotor.

As a consequence of the above definitions, the distribution function for ring polymer configurations to be inserted (eq 35) corresponds to that of isolated ring polymers interacting with the external potential U_{SF}. These configurations can be straightforwardly obtained by sampling them from a *NVT* path integral Monte Carlo simulation performed concurrently with the main calculation.

Finally, given our choice for $I_{N\to N+1}$, the ratio between the acceptance probabilities $A_{N\to N+1} = W_{N\to N+1}/I_{N\to N+1}$ of these insertion moves becomes

$$\frac{A_{N\to N+1}}{A_{N+1\to N}} = \frac{1}{N+1}\exp[\beta(\mu - \tilde{\mu})] e^{-\beta\Delta U_{FF}} \qquad (37)$$

Notice that eqs 36 and 37 above replace eqs 20−22 of the original BB paper,[10] where spurious factors of V and Λ^3 were incorrectly inserted. Notice, moreover, that eq 37 has the correct limit for the case of point particles in the absence of adsorbent (*i.e.*, $q_{rot} = 1$ and $U_{SF} = 0$). In that case, one has that $Q_{ads} = e^{-\beta\tilde{\mu}} = V/\Lambda^3$ (the ideal gas partition function) and the formula for the acceptance probabilities reduces to the one reported by Wang *et al.*[32]

In the following calculations, the insertion moves have been accepted using the standard Metropolis recipe

$$A_{N\to N+1} = \min\left[1, \frac{1}{N+1}\exp[\beta(\mu - \tilde{\mu})] e^{-\beta\Delta U_{FF}}\right] \qquad (38)$$

$$A_{N+1\to N} = \min[1, (N+1)\exp[-\beta(\mu - \tilde{\mu})] e^{\beta\Delta U_{FF}}] \qquad (39)$$

Potential Model. In order to assess the importance of quantized rotation on the selectivity, we need a potential model that explicitly treats the hydrogen molecule as a rigid rotor. To the best of our knowledge, no such model has been extensively tested in the literature, although we point out that recently, while this work was in preparation, an improved H_2-H_2 potential suitable for condensed state simulations has been developed.[45]

The zero-pressure selectivities of various H_2 potential models in the (3,6) nanotube have been evaluated in the framework of the "simple theory", that is, using eq 2 with the energy levels obtained by a direct diagonalization of the Hamiltonian,[8] as well as using suitable approximations valid under the conditions of strong confinement.[9] Many models predict very high selectivities (in the range of 10^7-10^{10}). However, the selectivity depends strongly on the potential parameters.

In this paper, we describe the hydrogen molecule as a rigid rotor of length $l = 0.74$ Å with two Lennard-Jones sites on the position of the hydrogen atoms, having as parameters $\varepsilon = 8.4$ K and $\sigma = 2.81$ Å.[46] It has been shown[8,9] that this model is able to describe the most relevant features of hydrogen adsorption in narrow carbon nanotubes, such as the very high isotopic selectivity and the related extreme 2D confinement regime.

The carbon atoms in the nanotubes are described with a Lennard-Jones potential, using the Steele parameters $\sigma_C = 3.4$ Å and $\varepsilon_C = 28.0$ K.[47] Solid−fluid interactions have been calculated using the Lorentz−Berthelot mixing rules. We have generated carbon nanotubes of various sizes and tabulated the solid−fluid potential by averaging over the angular coordinates and over the length of a unit cell in the direction z of the tube axis, thus obtaining the solid−fluid potential as a function of the distance of the molecule's site from the nanotube axis only.

In this study, we have focused our attention on the (3,6), (2,8), and (6,6) SWNTs. These tubes have geometrical radii of approximately 3.1, 3.6, and 4.1 Å, respectively. We report the profile of the potential energy with one of the hydrogen sites in Figure 7.

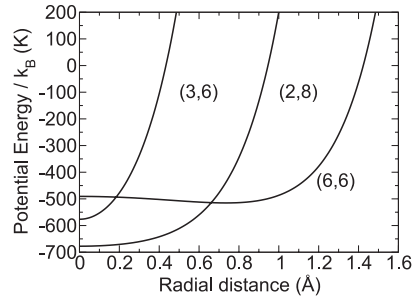

Figure 7. Average potential energy curves for one of the hydrogen sites with the carbon nanotubes used in this study, as a function of the distance from the tube axis.

REFERENCES AND NOTES

1. Beenakker, J. J. M.; Borman, V. D.; Krylov, S. Y. Molecular Transport in Subnanometer Pores: Zero-Point Energy, Reduced Dimensionality and Quantum Sieving. *Chem. Phys. Lett.* **1995**, *232*, 379–382.
2. Wang, Q.; Challa, S. R.; Sholl, D. S.; Johnson, J. K. Quantum Sieving in Carbon Nanotubes and Zeolites. *Phys. Rev. Lett.* **1999**, *82*, 956–959.
3. Challa, S. R.; Sholl, D. S.; Johnson, J. K. Light Isotope Separation in Carbon Nanotubes through Quantum Molecular Sieving. *Phys. Rev. B* **2001**, *63*, 245419.
4. Challa, S. R.; Sholl, D. S.; Johnson, J. K. Adsorption and Separation of Hydrogen Isotopes in Carbon Nanotubes: Multicomponent Grand Canonical Monte Carlo Simulations. *J. Chem. Phys.* **2002**, *116*, 814–824.
5. Hathorn, B. C.; Sumpter, B. G.; Noid, D. W. Contribution of Restricted Rotors to Quantum Sieving of Hydrogen Isotopes. *Phys. Rev. A* **2001**, *64*, 022903.
6. Trasca, R. A.; Kostov, M. K.; Cole, M. W. Isotopic and Spin Selectivity of H_2 Adsorbed in Bundles of Carbon Nanotubes. *Phys. Rev. B* **2003**, *67*, 035410.
7. Lu, T.; Goldfield, E.; Gray, S. K. Quantum States of Molecular Hydrogen and Its Isotopes in Single-Walled Carbon Nanotubes. *J. Phys. Chem. B* **2003**, *107*, 12989–12995.
8. Lu, T.; Goldfield, E.; Gray, S. K. Quantum States of Hydrogen and Its Isotopes Confined in Single-Walled Carbon Nanotubes: Dependence on Interaction Potential and Extreme Two-Dimensional Confinement. *J. Phys. Chem. B* **2006**, *110*, 1742–1751.
9. Garberoglio, G.; DeKlavon, M. M.; Johnson, J. K. Quantum Sieving in Single Walled Carbon Nanotubes: Effect of Interaction Potential and Rotational−Translational Coupling. *J. Phys. Chem. B* **2006**, *110*, 1733–1741.
10. Garberoglio, G. Boltzmann Bias Grand Canonical Monte Carlo. *J. Chem. Phys.* **2008**, *128*, 134109.
11. Kowalczyk, P.; Gauden, P. A.; Terzyk, A. P. Cryogenic Separation of Hydrogen Isotopes in Single-Walled Carbon and Boron-Nitride Nanotubes: Insight into the Mechanism of Equilibrium Quantum Sieving in Quasi-One-Dimensional Pores. *J. Phys. Chem. B* **2008**, *112*, 8275–8284.
12. Sandler, Y. L. The Adsorption and Ortho-Para Conversion of Hydrogen on Diamagnetic Solids. II. The Relative Adsorbabilities of Orthohydrogen and Parahydrogen. *J. Phys. Chem.* **1954**, *8*, 58–61.
13. Cunningham, C. M.; Johnston, H. L. The Surface Catalysis of the Ortho- to Para-Conversion in Liquid Hydrogen by Paramagnetic Oxides on Alumina. *J. Am. Chem. Soc.* **1958**, *80*, 2377–2382.
14. Cunningham, C. M.; Chapin, D. S.; Johnston, H. L. Separation of Orthohydrogen from Parahydrogen and of Paradeuterium from Orthodeuterium by Preferential Adsorption. *J. Am. Chem. Soc.* **1958**, *80*, 2382–2384.
15. Evett, A. A. Hindered Rotator Model for Adsorbed Hydrogen at Low Temperatures. *J. Chem. Phys.* **1959**, *31*, 565–566.
16. White, D.; Lassettre, E. N. Theory of Ortho-Para Hydrogen Separation by Adsorption at Low Temperatures, Isotope Separation. *J. Chem. Phys.* **1960**, *32*, 72–84.
17. Katorski, A.; White, D. Theory of Adsorption of the Isotopic Hydrogen Molecules at Low Temperatures. *J. Chem. Phys.* **1964**, *40*, 3183–3194.
18. Moiseyev, N. Isotope Effect on Physical Adsorption on a Non-Homogeneous Surface. *J. Chem. Soc., Faraday Trans. 1* **1975**, *71*, 1830–1837.
19. Kowalczyk, P.; Gauden, P. A.; Terzyk, A. P.; Bhatia, S. K. Thermodynamics of Hydrogen Adsorption in Slit-like Carbon Nanopores at 77 K. Classical *versus* Path Integral Monte Carlo Simulations. *Langmuir* **2007**, *23*, 3666–3672.
20. Kowalczyk, P.; Gauden, P. A.; Terzyk, A. P.; Furmaniak, S. Impact of the Carbon Pore Size and Topology on the Equilibrium Quantum Sieving of Hydrogen Isotopes at Zero Coverage and Finite Pressures. *J. Phys.: Condens. Matter* **2009**, *21*, 144210.
21. Wang, Y.; Bhatia, S. K. Simulation of Quantum Separation of Binary Hydrogen Isotope Mixtures in Carbon Slit Pores. *Mol. Simul.* **2009**, *35*, 162–171.
22. Garberoglio, G. Quantum States of Rigid Linear Rotors Confined in a Slit Pore: Quantum Sieving of Hydrogen Isotopes and Extreme One Dimensional Confinement. *Eur. Phys. J. D* **2009**, *51*, 185–191.
23. Hattori, Y.; Tanaka, H.; Okino, F.; Touhara, H.; Nakahigashi, Y.; Utsumi, S.; Kanoh, H.; Kaneko, K. Quantum Sieving Effect of Modified Activated Carbon Fibers on H_2 and D_2 Adsorption at 20 K. *J. Phys. Chem. B* **2006**, *110*, 9764–9767.
24. Bondarenko, S. D.; Alekseev, I. A. In *Hydrogen Materials Science and Chemistry of Carbon Nanomaterials*; Veziroglu, T. N. , Ed.; Springer: Berlin, 2007; pp 493−497.
25. Noguchi, D.; Tanaka, H.; Kondo, A.; Kajiro, H.; Noguchi, H.; Ohba, T.; Kanoh, H.; Kaneko, K. Quantum Sieving Effect of Three-Dimensional Cu-Based Organic Framework for H_2 and D_2. *J. Am. Chem. Soc.* **2008**, *130*, 6367–6372.
26. Garberoglio, G. Quantum Sieving in Organic Frameworks. *Chem. Phys. Lett.* **2009**, *467*, 270–275.
27. Anil Kumar, A. V.; Bhatia, S. K. Quantum Effect Induced Reverse Kinetic Molecular Sieving in Microporous Materials. *Phys. Rev. Lett.* **2005**, *95*, 245901.
28. Anil Kumar, A. V.; Bhatia, S. K. Erratum: Quantum Effect Induced Reverse Kinetic Molecular Sieving in Microporous Materials. *Phys. Rev. Lett.* **2006**, *96*, 119901.
29. Anil Kumar, A. V.; Jobic, H.; Bhatia, S. K. Quantum Effects on Adsorption and Diffusion of Hydrogen and Deuterium in Microporous Materials. *J. Phys. Chem. B* **2006**, *110*, 16666–16671.
30. Anil Kumar, A. V.; Bhatia, S. K. Is Kinetic Molecular Sieving of Hydrogen Isotopes Feasible. *J. Phys. Chem. C* **2008**, *112*, 11421–11426.
31. Chen, B.; Zhao, X.; Putkham, A.; Hong, K.; Lobkovsky, E. B.; Hurtado, E. J.; Fletcher, A. J.; Thomas, K. M. Surface Interactions and Quantum Kinetic Molecular Sieving for H_2 and D_2 Adsorption on a Mixed Metal-Organic Framework Material. *J. Am. Chem. Soc.* **2008**, *130*, 6411–6423.
32. Wang, Q.; Johnson, J. K.; Broughton, J. Q. Path Integral Grand Canonical Monte Carlo. *J. Chem. Phys.* **1997**, *107*, 5108–5117.
33. Xu, M.; Sebastianelli, F.; Bačic, Z.; Lawler, R.; Turro, N. J. Quantum Dynamics of Coupled Translational and Rotational Motions of H_2 Inside C_{60}. *J. Chem. Phys.* **2008**, *128*, 011101.
34. Xu, M.; Sebastianelli, F.; Gibbons, B. R.; Bačic, Z.; Lawler, R.; Turro, N. J. Coupled Translation-Rotation Eigenstates of H_2 in C_{60} and C_{70} on the Spectroscopically Optimized Interaction Potential: Effects of Cage Anisotropy on the Energy Level Structure and Assignments. *J. Chem. Phys.* **2009**, *130*, 224306.
35. Mamone, S.; Ge, M.; Hüvonen, D.; Nagel, U.; Danquigny, A.; Cuda, F.; Grossel, M. C.; Murata, Y.; Komatsu, K.; Levitt, M. H.; Room, T.; Carravetta, M. Rotor in a Cage: Infrared Spectroscopy of an Endohedral Hydrogen-Fullerene Complex. *J. Chem. Phys.* **2009**, *130*, 081103.
36. Landau, D. P.; Binder, K. *A Guide to Monte Carlo Simulations in Statistical Physics*; Cambridge University Press: New York, 2000; Chapter 8.
37. Marx, D.; Müser, M. H. Path Integral Simulations of Rotors: Theory and Applications. *J. Phys.: Condens. Matter* **1999**, *11*, R117–R155.
38. Müser, M. H. The Path Integral Monte Carlo of Rigid Linear Molecules in Three Dimensions. *Mol. Simul.* **1996**, *17*, 131–141.
39. Cui, T.; Cheng, E.; Adler, B. J.; Whaley, K. B. Rotational Ordering in Solid Deuterium and Hydrogen: A Path Integral Monte Carlo Study. *Phys. Rev. B* **1997**, *55*, 12253–12266.
40. Duane, S.; Kennedy, A. D.; Pendleton, B. J.; Roweth, D. Hybrid Monte Carlo. *Phys. Lett. B* **1987**, *195*, 216–222.
41. Tuckerman, M. E.; Berne, B. J.; Martyna, G. J.; Klein, M. L. Efficient Molecular Dynamics and Hybrid Monte Carlo Algorithms for Path Integrals. *J. Chem. Phys.* **1993**, *99*, 2796–2808.

42. Tuckerman, M. E.; Berne, B. J.; Martyna, G. J. Reversible Multiple Time Scale Molecular Dynamics. *J. Chem. Phys.* **1992**, *97*, 1990–2001.
43. Matubayasi, N.; Nakahara, M. Reversible Molecular Dynamics for Rigid Bodies and Hybrid Monte Carlo. *J. Chem. Phys.* **1999**, *110*, 3291–3301.
44. Miura, S. Rotational Fluctuation of Molecules in Quantum Clusters. I. Path Integral Hybrid Monte Carlo Algorithm. *J. Chem. Phys.* **2007**, *126*, 114308.
45. Belof, J. L.; Stern, A. C.; Space, B. An Accurate and Transferable Intermolecular Diatomic Hydrogen Potential for Condensed Phase Simulation. *J. Chem. Theory Comput.* **2008**, *4*, 1332–1337.
46. Murad, S.; Gubbins, K. E. Molecular Dynamics Simulations of Methane Using a Singularity Free Algorithm. In *Computer Modelling of Matter;* American Chemical Society: Washington, DC, 1978; Vol. 86, pp 62−71.
47. Steele, W. A. The Interaction of Rare Gas Atoms with Graphitized Carbon Black. *J. Phys. Chem.* **1978**, *82*, 817–821.